A linear relationship between ENSO intensity and tropical instability wave activity in the eastern Pacific Ocean

Jin-Yi Yu[1] and W. Timothy Liu[2]

[1] The interannual variations of tropical instability waves (TIWs) in the eastern Pacific Ocean and their relationships with ENSO intensity are studied using a 28-year long coupled atmosphere-ocean general circulation model (CGCM) simulation. The activity of TIWs is measured by the root-mean-square value of the 50-day high-pass filtered sea surface temperature (SST) perturbations produced in the simulation. The CGCM realistically produces two branches of large TIW activity near the equator: one at 2°N and the other at 2°S. It is found that along both branches there are linear relationships between the year-to-year variations of TIW activity and those of ENSO intensity. TIW activity is enhanced or reduced in proportion to the NINO3 SST anomalies, with larger activity in La Niña years and smaller activity in El Niño years. It is found that ENSO modulates TIW activity in both branches primarily by changing the latitudinal SST gradient associated with the SST front immediately north of the equator. Weaker correlations are found between the year-to-year variations of TIW activity and those of the ocean current shears between the south equatorial current and the equatorial undercurrent or the north equatorial countercurrent. This CGCM study suggests that the baroclinic instability associated with the northern SST front is a major generation mechanism for both the northern and southern TIW branches in the eastern Pacific Ocean. *INDEX TERMS:* 3339 Meteorology and Atmospheric Dynamics: Ocean/atmosphere interactions (0312, 4504); 4215 Oceanography: General: Climate and interannual variability (3309); 4522 Oceanography: Physical: El Niño; 1620 Global Change: Climate Dynamics (3309); 3374 Meteorology and Atmospheric Dynamics: Tropical meteorology. **Citation:** Yu, J.-Y., and W. T. Liu, A linear relationship between ENSO intensity and tropical instability wave activity in the eastern Pacific Ocean, *Geophys. Res. Lett.*, *30*(14), 1735, doi:10.1029/2003GL017176, 2003.

1. Introduction

[2] Tropical instability waves (TIWs) are cusp-shaped oceanic perturbations of currents and temperature and are often observed near the cold-tongue/InterTropical Convergence Zone (ITCZ) complex of the eastern Pacific Ocean [*Legeckis*, 1977]. The presence of TIWs has been linked to the barotropic instability of ocean current shears between the south equatorial current (SEC) and the equatorial undercurrent (EUC) or the north equatorial counter current (NECC) [e.g., *Philander*, 1978; *Cox*, 1980; *Qiao and Weisberg*, 1998] and the baroclinic instability of the sea surface temperature (SST) front immediately north of the equator [*Hansen and Paul*, 1984; *Yu et al.*, 1995]. Both instability mechanisms are closely tied to the thermodynamic structure of the cold-tongue/ITCZ complex in the eastern Pacific. TIW activity is therefore subject to modulation by the interannual variations of the complex: the El Niño-Southern Oscillation (ENSO). This study is aimed at examining the relationships between ENSO intensity and TIW activity in this region. Recent high-resolution observations from the TRMM Microwave Imager have revealed the existence of two distinct branches of TIWs in the eastern Pacific Ocean: one at 2°S and the other at 2°N [*Chelton et al.*, 2000]. This study contrasts the ENSO-TIW relationships in these two TIW branches to infer their generation mechanisms.

[3] In this study, a long-term simulation with a coupled atmosphere-ocean general circulation model (CGCM) is used. This methodology is adopted because in-situ measurements of TIWs are limited to fix locations [e.g., *Halpern et al.*, 1988; *Hayes et al.*, 1989] and are too sparse to provide a complete description of TIW activity and its variations. Satellite microwave measurements of SSTs can resolve TIW activity very well and have recently been used to examine the interannual variations of TIWs [*Contreras*, 2002]. But the length of the observations is still limited. The selection of a CGCM simulation for this study is further motivated by the recent findings that TIWs have significant couplings with the atmosphere [*Xie et al.*, 1998; *Liu et al.*, 2000; *Chelton et al.*, 2000; *Hashizume et al.*, 2001]. SST perturbations associated with TIWs are often accompanied by significant fluctuations in the atmosphere. For example, *Liu et al.* [2000] used satellite observations to show that warm (cold) SST centers of TIWs are often accompanied by strong (weak) surface wind and enhanced (reduced) evaporation in the atmosphere. They argued that the feedbacks from the atmosphere to the ocean may affect the development of TIWs. Therefore, CGCM simulations provide one useful way to examine the interannual variations of TIWs and their relationships with ENSO.

2. Model and Simulation

[4] The CGCM used in this study consists of the UCLA atmospheric GCM (AGCM) and the GFDL Modular Ocean Model (MOM) (see *Yu and Mechoso*, 2001 for a detailed description of the CGCM). The AGCM is global with a horizontal resolution of 5°-longitude by 4°-latitude and 15 levels in the vertical. The oceanic model has a longitudinal resolution of 1°, a latitudinal resolution that varies gradually from 1/3° between 10°S and 10°N to about 3° at both 30°S

---

[1]Department of Earth System Science, University of California, Irvine, CA, USA.
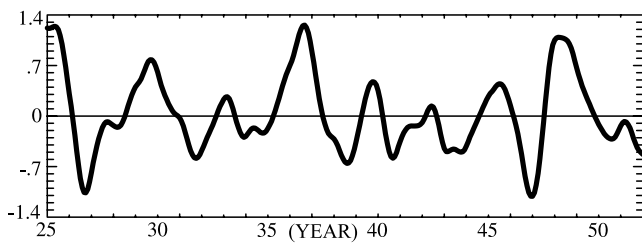[2]Jet Propulsion Laboratory, California Institute of Technology, Pasadena, CA, USA.

Figure 1. NINO3 SST anomalies calculated from the CGCM simulation.

Figure 2. The root mean square values of the 50-day high-pass filtered SST perturbations averaged during years 26–52 of the CGCM simulation. Contour intervals are 0.1°C. Values greater than 0.4 are shaded.

and 50°N, and 27 layers in the vertical. At these resolutions, the OGCM is capable of resolving TIWs that have typical wavelengths of 1000 km. Outside the oceanic model domain, SSTs for the AGCM are prescribed based on a monthly-varying SST climatology.

[5] A 53-year long simulation was performed with the CGCM by *Yu and Mechoso* [2001] to study the dynamics of the ENSO cycle. In the present study, only the last 28 years (years 25–52) of the simulation are used to analyze the ENSO-TIW relationships. *Yu and Mechoso* [2001] showed that this CGCM simulation produces ENSO-like interannual variability, which is characterized by predominantly standing oscillations of SST in the eastern Pacific. Figure 1 shows the interannual variations of SST anomalies in the NINO3 region (90°W–150°W; 5°S–5°N) for years 25–52 of the simulation. The values shown are the departures of the simulated SSTs from the long-term mean annual cycle. A low-pass filter is applied to the departures to retain only the variability with timescales longer than one year. Figure 1 shows that ENSO-like events are produced in the simulation approximately every 3–4 years, with the largest NINO3 anomalies close to 1.4°C. The standard deviation of the simulated NINO3 index is about 0.6°C, which is close to the observed values of 0.7°C estimated from *Kaplan et al.* [1998] dataset.

3. Simulated Tropical Instability Waves

[6] TIWs are observed to have dominant time scales of 20–40 days [e.g., *Qiao and Weisberg*, 1995]. The 3-day mean SSTs output from the CGCM simulation are high-pass filtered by a recursive filter to keep only the variations with timescales shorter than 50 days. We calculate the root mean square (RMS) of the filtered SST anomalies to measure TIW activity. Figure 2 shows the spatial distribution of the RMS calculated from years 25–52 of the simulation. It shows that the CGCM produces two distinct branches of strong TIW activity in the Pacific Ocean: One at 2°N and the other at 2°S. The northern branch is centered more in the eastern Pacific and has larger values than the southern branch, which has its largest values in the central Pacific. The location and the relative strength of these two simulated TIW branches are similar to those observed by the TRMM Microwave Imager during 1998–1999 [*Chelton et al.*, 2000]. The simulated TIWs also show large seasonal and interannual variations. Figure 3 illustrates some of those variations by showing the filtered SST anomalies along the northern TIW branch from years 26 to 30. Large TIW signals propagate westward over the central-to-eastern Pacific from July to December of all model years. There
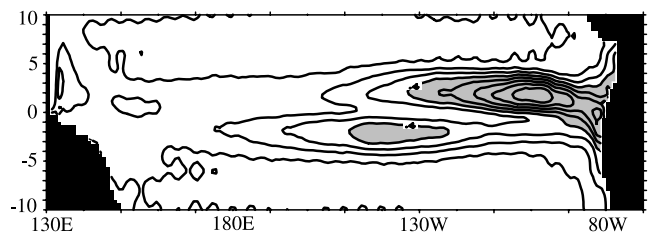
is almost no TIW signal during January–June of each year. During a cold ENSO year (year 26; see Figure 1), TIW signals are particularly strong and are extend further westward. During a warm ENSO year (year 29), TIW signals are weak and more confined to the eastern Pacific. The variations of the southern TIW branch are similar to those of the northern branch, except that the southern branch tends to peak during May–October in the simulation. The analyses performed in the rest of this study only use data from the July–December period of every model year to focus on TIW activity.

4. Interannual Variations

[7] We have shown in Figure 3 that TIW activity is suppressed during warm ENSO years and is enhanced during cold ENSO years, which is consistent with the observations [e.g., *Contreras*, 2002]. To further examine the relation between ENSO intensity and TIW activity, Figure 4a shows the year-to-year variations of the mean activity of the northern and southern TIW branches and their relationships with NINO3 SST anomalies. Here the TIW activity is represented by the root mean square of filtered SST perturbations averaged along the northern
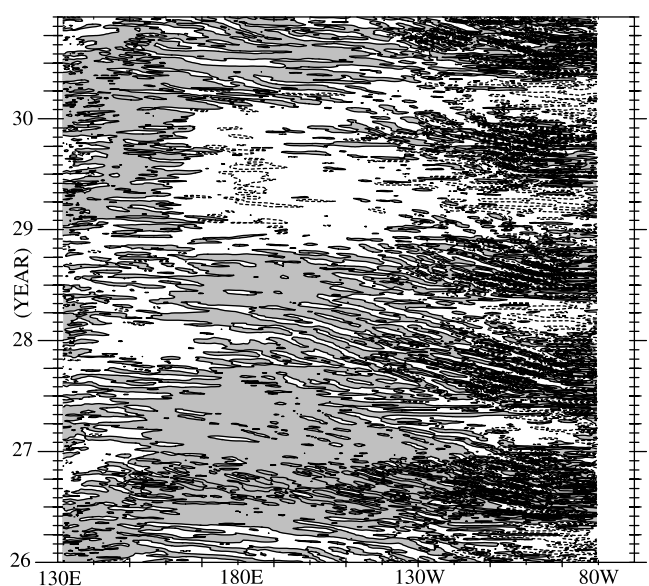

Figure 3. Time-longitude section of the filtered SST perturbations produced by the CGCM along 2°N. Contour intervals are 0.5°C.
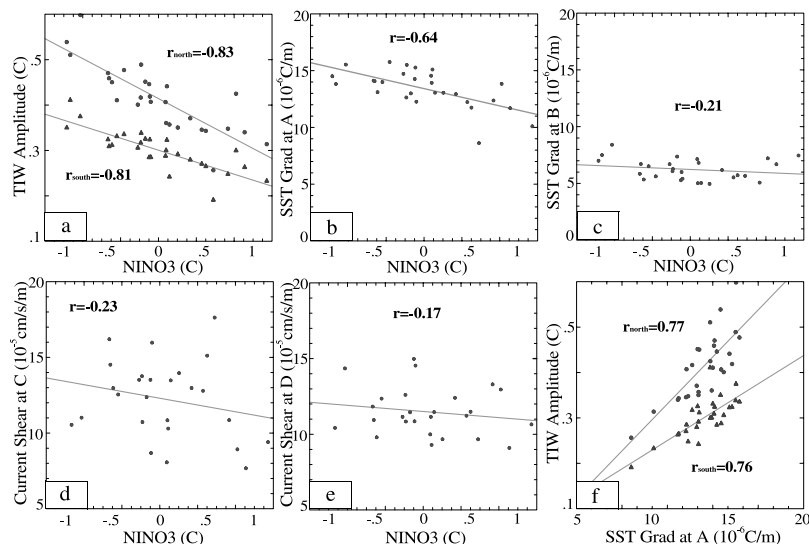
Figure 4. Scattering plots showing the year-to-year relationships between ENSO intensity and (a) TIW amplitudes at the northern (circle) and southern (triangle) branches, (b) latitudinal gradient of the northern SST front (box "A" of Figure 5), (c) latitudinal gradient of the southern SST front (box "B"), (d) latitudinal shear between the EUC and the SEC (box "C"), and (e) latitudinal shear between the SEC and the NECC (box "D"). Panel (f) is the relationship between the latitudinal gradient of the northern SST front and the TIW amplitudes along the northern (circle) and southern (triangle) branches. The least square fits to these relationships are also shown. The correlation coefficient (r) of each pair of the time series is indicated in each panel.

(2°N) and southern (2°S) TIW branches from 130 E to 80 W and from July to December of each model year. ENSO intensity is represented by the interannual NINO3 SST anomalies averaged during the same period. The most striking feature in Figure 4a is the near-linear relationships between TIW activity and ENSO intensity for both TIW branches. This figure shows that the northern TIW branch experiences slightly larger interannual variations than the southern TIW branch. This is evident from the larger slope of the least square fit for the northern branch (slope = −0.10) than that for the southern branch (slope = −0.06). We also performed similar analyses (not shown) of the TIW activity averaged over wider latitudinal bands (1°N−8°N for the northern branch; 1°S−8°S for the southern branch) and find similar linear relationships.

[8] This linear modulation by ENSO of the TIW activity must be achieved through the instability mechanisms that generate TIWs: either the baroclinic instability associated with the SST fronts or the barotropic instability associated with the ocean current shears between the SEC and the EUC or the NECC. To infer the primary mechanism that allows ENSO to modulate TIW activity, we first examine how the SST gradients and current shears associated with these instability mechanisms change with ENSO intensity. Figure 5 displays the mean thermodynamic structure of the eastern Pacific Ocean simulated by the CGCM during July–December. Figure 5a shows that the mean SST simulated by the CGCM has two large SST fronts in the eastern Pacific Ocean: One along 2°N and the other along 2°S. We use two SST gradient indices calculated from two sectors of these two fronts (marked as "A" and "B" in Figure 5a) to represent the strength of their associated baroclinic instabilities. Figure 5b displays the latitude-depth structure of the simulated zonal currents averaged between 130 W and 80°W. Two current shear indices are selected to represent

the shear between the SEC and the EUC (marked as "C" in Figure 5b) and the shear between the SEC and the NECC (marked as "D" in Figure 5b). These four gradient/shear indices are selected to measure the strength of the baroclinic and barotropic instabilities in the region.

[9] The year-to-year relationships between ENSO intensity and the shear/gradient indices are shown in Figures 4b−4e. The shear/gradient values shown here are the magnitudes (i.e., the absolute values) and are scaled by a factor of 1×10^6 and 1×10^5, respectively, for SST
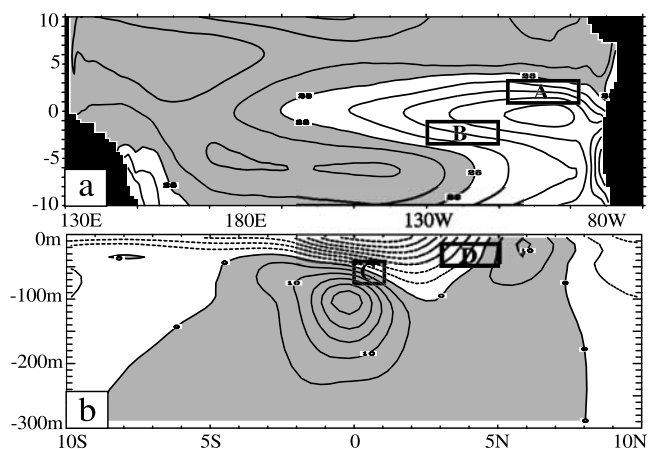

Figure 5. The mean thermodynamic structure of the cold tongue-ITCZ complex simulated by the CGCM during the July–December season. Panel (a) shows the mean SSTs and (b) shows the latitude-depth structure of the mean zonal currents averaged between 120°W−80°W. Contour intervals are 2°C for (a) and 5 cm/sec for (b). Values greater than 28°C are shaded in (a). Eastward currents are also shaded.

gradients and current shears. It is apparent from Figures 4b–4e that, among all the four indices, ENSO intensity affects the latitudinal gradient of the northern SST front (box "A" of Figure 5) the most. The northern SST gradient increases and decreases in proportion to ENSO intensity, with larger values in La Niña years and smaller values in El Niño years. The correlation coefficient of this index with the NINO3 index is the largest (−0.64) among all indices and is significant at the 99.9% level. The SST gradient of the southern SST front ("B") is also affected by ENSO intensity, but the changes in gradient are relatively small. The shears between the SEC and EUC (Figure 4d) and the shear between the SEC and the NECC (Figure 4e) show weaker tendency to have a linear relationship with ENSO intensity, as indicated by the large deviations of the points from the least square fit and small correlation coefficients.

[10] The correlation analysis shown in Figure 4 suggests that ENSO intensity has a strong influence on the latitudinal gradient of SST front immediately north of the equator. We next ask how TIW activity responds to the changes of the northern SST gradient. Figure 4f shows that the year-to-year relationships between the latitudinal gradient of the northern SST front and the TIW activity along the two TIW branches. It shows linear relationships between the SST gradient and the TIW activity of both branches. Therefore, our correlation analysis suggests that ENSO events modulate the activity of both TIW branches by changing the latitudinal gradient of the SST immediately north of the equator. This result suggests that the baroclinic instability associated with the northern SST front is a major generation mechanism to both the northern and southern branches of TIWs in the eastern Pacific.

5. Summary and Discussion

[11] This study uses a long-term CGCM simulation to examine the interannual variations of TIW activity in the eastern Pacific and their relationships with ENSO intensity. This CGCM is shown to produce a realistic simulation of TIWs, including their seasonal and interannual variations and the two branches of high TIW activity. We focus on quantifying the relationship between ENSO intensity and the interannual variations of TIW intensity along the northern and southern TIW branches. Near-linear relationships are found between ENSO intensity and the TIW activity of both branches. TIW activity increases during La Niña years and are reduced during El Niño years, in proportional to the NINO3 SST anomalies. We use the linear TIW-ENSO relationships to infer the generation mechanisms for the northern and southern TIW branches. Our correlation analysis suggests that both the northern and southern TIW branches are modulated by ENSO through the SST gradient immediately north of the equator. It is noted that the strength of the simulated equatorial undercurrent is weaker than the observed (Figure 5b). This may (or may not) allow the baroclinic instability mechanism to become more dominant in the generation of TIWs in the simulation. Never-

theless, there are two major implications from this modeling study. The first is that the baroclinic instability associated with the northern SST front is a major generation mechanism to both the northern and southern TIW branches in the eastern Pacific Ocean. The second implication is that ENSO exerts a strong and linear modulation of the intensity of TIWs, which are known to play important roles in the heat budget of the eastern Pacific Ocean. How the subsequent changes in TIW-induced heat transports affect the thermo-dynamic structure of the ITCZ-cold tongue complex in the eastern Pacific Ocean and feedback to the ENSO cycle deserves further study. The near-linear relationships between ENSO intensity and TIW activity obtained from this investigation provide a framework for such studies.

References

Chelton, D. B., F. J. Wentz, C. L. Gentemann, R. A. de Szoeke, and M. G. Schlax, Satellite microwave SST observations of transequatorial tropical instability waves, *Geophys. Res. Lett.*, *27*, 1239–1242, 2000.

Contreras, R. F., Long-term observations of tropical instability waves, *J. Phys. Oceanogr.*, *132*, 2715–2722, 2002.

Cox, M. D., Generation and propagation of 30-day waves in a numerical model of the Pacific, *J. Phys. Oceanogr.*, *10*, 1168–1186, 1980.

Halpern, D., R. Knox, and D. S. Luther, Observations of 20-day period meridional current oscillations in the upper ocean along the Pacific Equator, *J. Phys. Oceanogr.*, *18*, 1514–1534, 1988.

Hansen, D. V., and C. A. Paul, Genesis and effects of long waves in the equatorial Pacific, *J. Geophys. Res.*, *89*, 10,431–10,440, 1984.

Hashizume, H., S.-P. Xie, W. T. Liu, and K. Takeuchi, Local and remote atmospheric response to tropical instability waves: a global view from space, *J. Geophys. Res.*, *106*, 10,173–10,185, 2001.

Hayes, S.-P., M. J. McPhaden, and J. M. Wallace, The influence of sea surface temperature upon surface wind in the eastern equatorial Pacific: Weekly to monthly variability, *J. Climate*, *2*, 1,500–1,506, 1989.

Kaplan, A., M. Cane, Y. Kushnir, A. Clement, M. Blumenthal, and B. Rajagopalan, Analyses of global sea surface temperature 1856–1991, *J. Geophys. Res.*, *103*, 18,567–18,589, 1998.

Legeckis, R., Long waves in the eastern equatorial Pacific: A view of a geostationary satellite, *Science*, *197*, 1,177–1,181, 1977.

Lui, W. T., X. Xie, P. S. Polito, S.-P. Xie, and H. Hashizume, Atmospheric manifestation of tropical instability wave observed by QuikSCAT and Tropical Rain Measuring Mission, *Geophys. Res. Lett.*, *27*, 2534–2548, 2000.

Philander, S. G. H., Instabilities of zonal equatorial currents, 2, *J. Geophys. Res.*, *83*, 3,679–3,682, 1978.

Qiao, L., and R. H. Weisberg, Tropical instability wave kinematics: Observations from the tropical Instability Wave Experiment, *J. Geophys. Res.*, *100*, 8,677–8,693, 1995.

Xie, S.-P., M. Ishiwatari, H. Hashizume, and K. Takeuchi, Coupled ocean-atmospheric waves on the equatorial front, *Geophys. Res. Lett.*, *25*, 3863–3866, 1998.

Yu, J.-Y., and C. R. Mechoso, A coupled atmosphere-ocean GCM study of the ENSO cycle, *J. Climate*, *14*, 2,329–2,350, 2001.

Yu, Z., J. P. McCreary, and J. A. Proehl, On the meridional asymmetry and energetics of tropical instability waves, *J. Phys. Oceanogr.*, *25*, 2,997–3,007, 1995.

———————
J.-Y. Yu, Department of Earth System Science, University of California, Irvine, USA. (jyyu@uci.edu)

W. T. Lui, Jet Propulsion Laboratory, California Institute of Technology, USA. (lui@pacific.jpl.nasa.gov)